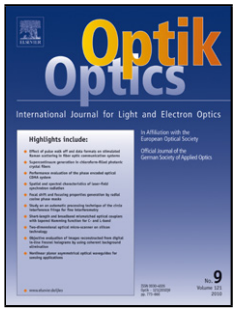


Title: Nonlinear characterization of conducting polymer and electrical study for application as solar cells and its antibacterial activity

Author: Hussain A. Badran Hussain F. hussain Khalid I. Ajeel

PII: S0030-4026(16)30198-X
DOI: http://dx.doi.org/doi:10.1016/j.ijleo.2016.03.030
Reference: IJLEO 57427

To appear in:

Received date: 30-1-2016
Accepted date: 7-3-2016

Please cite this article as: H.A. Badran, H.F. hussain, K.I. Ajeel, Nonlinear characterization of conducting polymer and electrical study for application as solar cells and its antibacterial activity, *Optik - International Journal for Light and Electron Optics* (2016), http://dx.doi.org/10.1016/j.ijleo.2016.03.030

# Nonlinear characterization of conducting polymer and electrical study for application as solar cells and its antibacterial activity

Hussain A. Badran*, Hussain F. hussain and Khalid I. Ajeel

Basrah University, College of Education for Pure Sciences, Department of Physics, Basrah, Iraq.

*Corresponding Author Email: badran_hussein@yahoo.com

**Abstract**

A conducting polymer, Poly (O- Methoxyaniline) (POMA), has been synthesized by the chemical polymerization and characterized by FT-IR, AFM, Raman, and an UV–visible spectrometer. Measurements of the thermally induced optical nonlinearity of POMA thin film and orcein dye in a N-methyl-2-pyrrolidone (NMP) solvent were studied using a cw diode laser at 532 nm as the source of excitation, both in solution and as a POMA solid film, respectively. The optical response was characterized by measuring the intensity-dependent refractive index $n_2$ of the medium using the Z-scan technique. The optical properties of the thin films prepared were studied including recording the absorption spectroscopy for wavelengths of (300-900nm). The absorption coefficient and the forbidden energy gap to transmission directly were measured as well as the refraction index, $n$, extinction coefficient , $k$, dielectric constant ε. The optical constant represented by single oscillator energy, $E_0$, dispersion energy, $E_d$, moment of dielectric constant ($M_{-1}, M_{-3}$), nonlinear optical susceptibility, $\chi^3$,were determined. For the electronic application of prepared polymers POMA a solar cells were constructed by using n-type silicon wafers and different electrode from gold and aluminium. The electrical properties of the solar cell under the effect of the light equivalent to that of the sun and which falls vertically on the sample were studied. It is practically found that, the conversion efficiency is 0.4%. A better antibacterial activity was observed against Staphylococcus aureus (SA), Escherichia coli (EC), Streptococcus pyogenes, Klebsiella pneumoniae, and Proteus mirabilis by conducting polymer POMA thin film.

Keywords: solar cell; efficiency; z-scan; electrical properties.

## 1. Introduction

Renewable energy is basically the energy that comes from natural sources directly or can be derived from these natural sources. Unlike fossil fuels, which are exhaustible, renewable energy sources regenerate constantly and can be sustained indefinitely [1,2]. With a steady improvement in energy conversion efficiency during the past decades, organic photovoltaic (OPV) has evolved into a promising technology for renewable energy made possible by the first report of planar donor–acceptor

heterojunction. Organic bulk heterojunction (BHJ-OPV) photovoltaics are solar cells that employ organic materials, either polymers (macromolecules) or small molecules, to absorb light and produce free electrons [3-5]. Polymer materials have attracted the scientific technological researchers, this is mainly due to their wide industrial applications. Conducting polymrrs (CPs) have a great potential in many important branch of material science owing to many applications in electronics and photonics. According to their unique properties such as low density, ability to form intricate shapes. Versatile electric properties and low manufacturing cost polymers coating have shown optical properties, which are highly promising for opto-electronics applications. Fabrication of high performance electrical or opto-electrical devices, such as light emitting diodes, all polymer transistors, laminated photovoltaic diodes, solar cells. Many potential applications of conducting polymers (CPs) are limited because of their general insolubility in common organic solvents, insufficient environmental stability and poor mechanical properties. As away to improve processability and atmospheric stability one method is to prepare composites of conducting polymers and processable non-conducting polymers. One way of Synthesizing these composites involved making the conducting polymer inside the matrices of conventional polymers using chemical method for polymerization. They also have potential advantages for applications in optical storage systems, such as high thermal stability, low absorption loss, and the ability of refractive index change upon exposure to light [5]. The electrical and optical properties of polymers have attracted much attention in view of their applications in optical devices with remarkable reflection, antireflection interference and polarization properties. Recently, electrical conductivity of polyaniline doped PVC-PMMA polymer blend, Deshmukh et al [6].

In this work a synthesis of POMA thin film deposited on either silicon or glass microslide using spin coating technique and study the optical and photovoltaic properties of prepared film. The optical properties will include transmittance, absorbance, reflectance, optical constants, energy band gap and refractive index dispersion as well as the present study included the construct and study organic material on inorganic thin films solar cell structures. polymeric solar cell have attracted great attention due to the advantages of light weight, flexibility and low cost with the possibility of fabricating large area device by cheaper liquid based process. However the power conversion of organic solar cell is limited by the low dissociation probability of excitons and inefficient hopping carrier transport [7]. Also an attempt has been made to study the antibacterial activity against Staphylococcus aureus (SA), Escherichia coli (EC), Streptococcus pyogenes, Klebsiella pneumoniae, and Proteus mirabilis for conducting polymer POMA thin films. The nonlinear refraction index $n_2$ and the nonlinear absorption coefficient $\beta$ of the dye were studied with a cw diode laser with an output power of 40 mW at 532 nm using the Z-scan technique, based on the sample-induced changes in a beam profile at the far field.

## 2 . Experimental

The polymer POMA films were prepared by chemical method then dried in an oven at 50 $^0$C for 48 hrs. Powder of this polymer was dissolved in formic acid (HCOOH) with concentration of 10 mg/L and then the polymer deposited on either glass or silicon wafers substrates by spin coating method with different speed 1000, 2000, 3000, 4000 and 5000 rpm for thickness 124.5, 87.66, 74, 72 and 35nm respectively. The samples were put on hotplate to various the temperature from room temperature to 90 $^0$C. The measurement was carried out using digital thermometer. The spectroscopic ellipsometry has been used to determine the film thickness and the optical constant of spun POMA films, is a very sensitive, non destructive experimental technique of thin film characterization. Spectroscopic ellipsometry measurement on film deposited onto silicon (Si) or glass substrate were performed by using a variable angle spectroscopy ellipsometer (VASEC) Woolam M-2000 Tm ellipsometer operating in the spectral range of the wavelength between 360nm and 1000nm. The angle of incident was fixed at the angle of 70 $^0$C.

The thicknesses of all films fall in the range of 124.5- 35 nm which is reasonable for film of polymers of similar nature formed under the same fabrication condition. Raman spectroscopy of POMA was employed to estimate the structural orientation of the polymer as shown in Fig.1, the benzene C-H bending deformation mode lies at 1120 and 1180 cm$^{-1}$ for the reduced semiquinone and quinoid ring structure. The band at 1260 cm$^{-1}$ can be assigned to the C–N stretching mode of the polaronic units. The band at 1340 cm$^{-1}$ corresponds to the C–N•+ stretching modes of the delocalized polaronic charge carriers while (C=C) stretching of the benzenoid ring was observed at 1600 cm$^{-1}$. A small peak positioned at 1450 cm corresponds to the C=N stretching mode of the quinoid units. A band of moderate intensity at 1500 cm corresponds to the bending deformation of the N•+ –H unit [8].

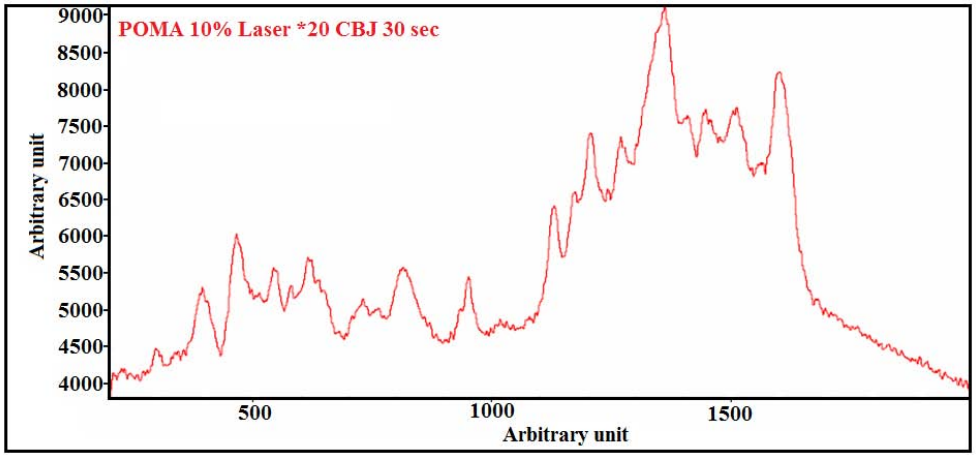


**Fig.1**. Raman spectra of POMA.

The POMA polymer was characterized by FTIR spectroscopy as a powder, the FTIR spectra Fig. 2 showed that the presence of the expected functional groups, for example the band at 3300 $cm^{-1}$ related to hydrogen bonding (NH), band at 2910 $cm^{-1}$ can be assigned to the stretching vibrat of the (-CH3) alphatic. The two bands appeared at (1590 $cm^{-1}$, and 1480 $cm^{-1}$) corresponding to the stretching vibration of the quinoid and benzenoid ring, respectively. The band at (1375 $cm^{-1}$) is due to the symmetric deformation of methyl group. The bands at (1320 $cm^{-1}$, and1210 $cm^{-1}$) can be assigned to the (C-N) mode. Whereas the bands at (1150 $cm^{-1}$, 1110 $cm^{-1}$, and 1105 $cm^{-1}$), are the characteristic bands of (C-H) bending vibration. The three bands appearing at (810 $cm^{-1}$, 880 $cm^{-1}$, and 940 $cm^{-1}$) were attributed to an out of plane (C-H)vibration of quinoid rings. The presence of bands at (1590$cm^{-1}$, and 1480 $cm^{-1}$) clearly shows that the polymer is composed of amine and imine units. The characteristic bands for the furetional group are different from these bands at 1450 $cm^{-1}$ corresponding to C-H bending of the $OCH_3$ and at 1000 $cm^{-1}$ to the C-O-C stretching of alkyl aryl ether linkage [9,10].

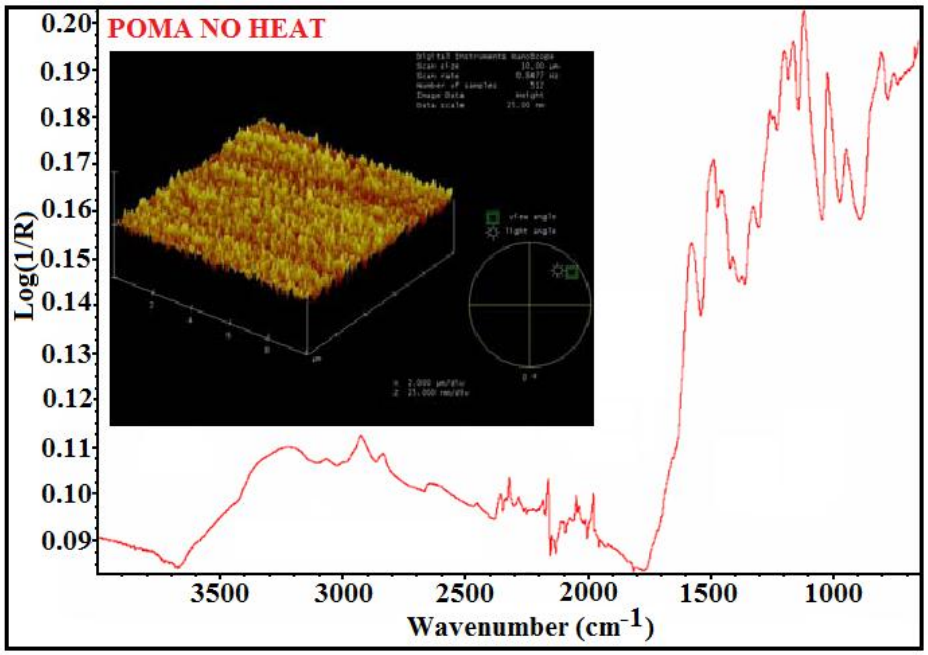


**Fig.2.** FT-IR spectra of POMA. *Inset* shows AFM image of POMA.

## 3. Results and Discussions:

Optical absorption coefficient , $\alpha$ , has been studied as a function of photon energy and the energy gap , $E_g$ , has been estimated. The dispersion parameters such as single oscillator energy, $E_0$ , dispersion energy, $E_d$ ,dielectric constant , $\varepsilon_\infty$ ,moment of dielectric constant optical spectrum ( $M_{-1}, M_{-3}$ ) and nonlinear optical susceptibility $\chi^3$ were studied as well .

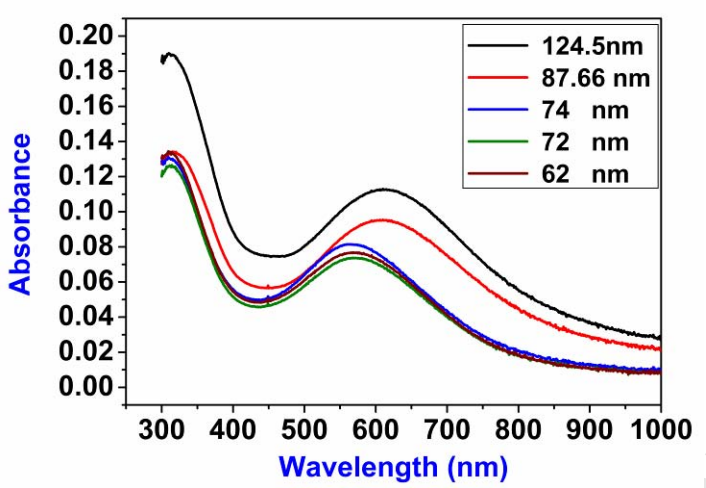


**Fig.3.** Optical absorption versus wavelength at different thickness of POMA.

Fig. 3 shows UV-Vis spectra of POMA with the different thickness. The first peak at about 300 nm (4.1eV), corresponding to the bonding to anti-bonding ($\pi - \pi^*$) transition of benzenoid rings, showed a hypsochromic shift, suggesting shorter conjugation length in the polymer chain, [11] consistent with the FTIR spectra. The second peak at about 600 nm (2.1eV) is assigned to the excitonic transition from the non-bonding to the anti-bonding orbital (n– $\pi^*$) between the highest occupied molecular orbital (HOMO) of the benzenoid ring (non-bonding nitrogen lone pair) and the lowest unoccupied molecular orbital (LUMO) of the quinonoid ring [12]. The second peak is a shift toward short wavelength as the thickness of the film increase, while the first peak did not change.

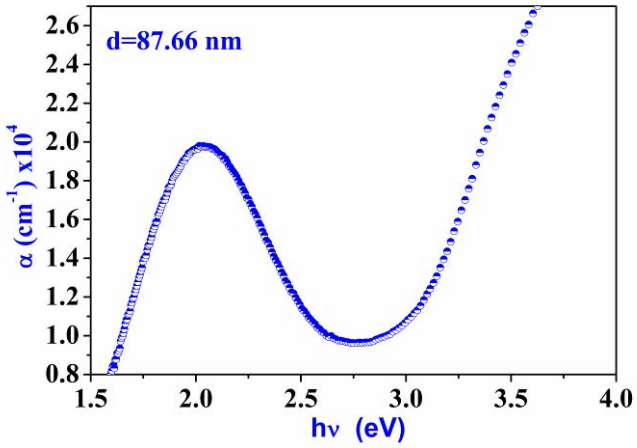


**Fig.4.** Absorption coefficients versus photon energy of POMA.

Fig.4 shows the relationship between absorption coefficient and photon energy of POMA polymer. The value of absorption coefficient plays an important role in the limitation of the type of transition. From the figures the value of the , $\alpha$, was greater than $10^4$ $cm^{-1}$ indicating that the transition was direct electron transmission. Semiconductors are generally classified into two types, direct and indirect gaps. In indirect band gap should always be associated with a phonon of the right value of crystal

momentum. Both direct and indirect transitions occurrence can be seen by plotting $(\alpha hv)^n$ as a function of photon energy $hv$ [13].

The band gap energy calculated by spectrophotometric data using following equation [14],

$$\alpha hv = B(hv - E_g)^r \quad (1)$$

Where $\alpha$ is the absorption coefficient , $h$ Planck's constant, vis the Frequency of incident light , $E_g$ is the optical band gap in eV, and $B$ is constant depended on type of material, $r$ Factor governing the direct/ indirect, etc. transitions of the electrons from the valence band to the conduction band. The variation of $(\alpha hv)^2$ with photon energy ($hv$) for the prepared films are shown in Fig. 5. The direct $E_g$ can be calculated from the intercept of the resulting straight lines with the energy axis at $(\alpha hv)^2 = 0$. It is found to be 3.22 eV.

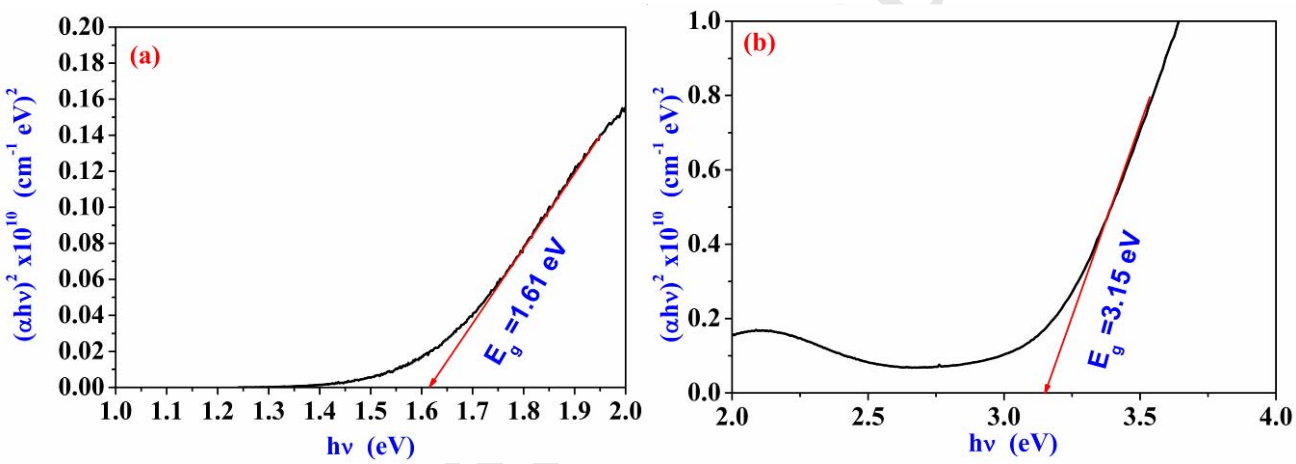


**Fig. 5.** Photon energy dependence of $(\alpha hv)^2$ for POMA film (a) first region, and (b) second region.

The direct optical band gap derived for the film is listed in Table 1. It is worth to mention that the fundamental gap''HOMO–LOMO gap'', $E_{gf}$, is the minimum energy formation of a separated, uncorrelated free electron and hole, and associated with the transport of single particles in the solid. The onset optical gap , $E_{go}$, on the other hand, corresponds to the onset of optical absorption and formation of a bound electron–hole pair, or exciton. $E_{gf}$ is larger than $E_{go}$ by a significant amount corresponding to the binding energy of the exciton $E_B$, the consensus from experimental results was obtained over the past few years with various techniques, as well as from theory, is that $E_B$ =0.5-1.5eV in molecular solid [15]. The magnitude of the obtainde values of $E_{gf}$ , $E_{go}$ are observed in Fig.5. In our

case, the allowed direct transition optical gap is found to be 1.61 eV and 3.15 eV, respectively for $E_{go}$ and $E_{gf}$. The optical properties of POMA thin film are essentially dependent on its refractive index, $n$, and extinction coefficient, $k$. Fig.6 shows the relationship between the optical parameters ($k, n$) as a function of wavelength. It can be seen from the figure that the parameters are increasing at low wavelength 540-600 nm. After that, the both parameter are decreasing while the $k$ parameter increases with increasing wavelength above 680 nm. The large value of $n$ indicated in that the compound is absorbing. The wavelength of the $n$ and $k$ parameters in investigated wavelength range shows that the same interaction occurs between photons and electrons. The refractive index changes with the variation of the wavelength of the incident light beam according to these interaction [16].

$$\alpha = 4\pi k / \lambda \qquad (2)$$

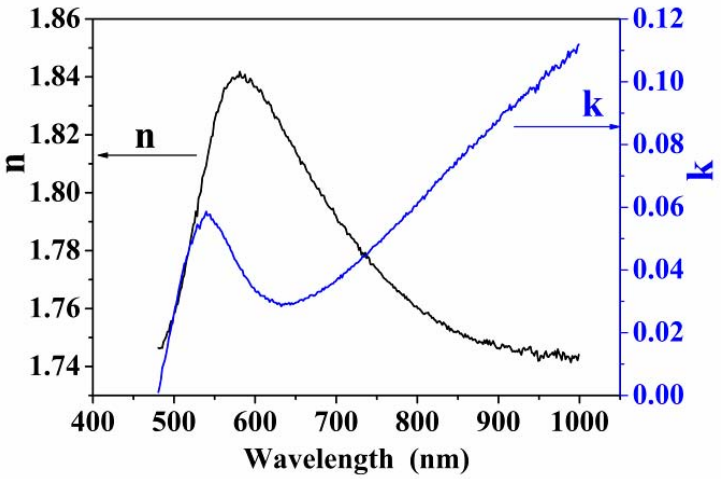


**Fig. 6.** Refractive index, $n$ and Extinction coefficient, $k$ as a function of wavelength for POMA.

**4. Dispersion Parameters**:

The dispersion data of the refractive index can be fitted to the Sellmeier-type dispersion model, which assumes that the composite materials are composed of individual dipole oscillators that are set to forced vibration by the incident light. The Sellmeier dispersion relation is given by [17,18]:

$$n^2(\lambda) - 1 = \sum_i \left( \frac{s_i \lambda_i^2}{1 - (\lambda_i / \lambda)^2} \right) \qquad (3)$$

where $S_i$ is the strength of the individual dipole oscillator and $\lambda_i$ is the oscillator wavelength. From Wemple and Di Domenico (WDD) proposition, the lowest energy oscillator has the largest contributor to n and the properties of the investigated materials could be treated as a single oscillator at

wavelength $\lambda_0$. Thus the dispersion of refractive index could be adequately described by a single term Sellmeier relation and Eq. 3 can simplified as follow [17]:

$$(n^2-1)^{-1} = \frac{E_0}{E_d} - \frac{1}{E_0 E_d} E^2 \quad (4)$$

or

$$n^2 - 1 = \left( \frac{S_0^2 \lambda_0^2}{1-(\lambda^2/\lambda_0^2)} \right) \quad (5)$$

where E(=hv) is the photon energy, $E_0$ is the oscillator energy and $E_d$ is the dispersion energy, *So* is the average oscillator strength which equals to:

$$S_0 = \frac{n_0^2 - 1}{\lambda_0^2} \quad (6)$$

A plot of $1/(n^2 -1)$ with $(hv)^2$ of the film at 87.66 nm thicknes are illustrated in Fig.7.

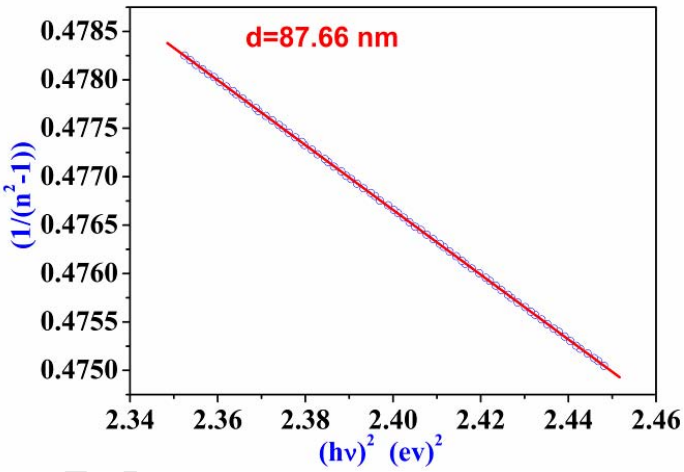


**Fig.7.** The $1/(n^2-1)$ versus $(hv)^2$ plot for POMA

The oscillator parameter $E_0$ and $E_d$ values were determined from the slope $(E_0\, E_d)^{-1}$ and intercept $(E_0/E_d)$ on the vertical axis respectively. The oscillator energy, $E_0$ is related to this optical band gap. Using the curve above the determined the value of the oscillator's parameters $E_0$ is 4.918 eV and $E_d$ is 10.03 eV. It is known that inter-material boundaries contain structural defects and impurities. These factors have a strong influence on the absorption process [19].

The $M_{-1}$ and $M_{-3}$ moments of the optical spectra can be obtained from the relationship [20,21]

$$E_o^2 = \frac{M_{-1}}{M_{-3}} \quad \text{and} \quad E_d^2 = \frac{M_{-1}^3}{M_{-3}} \quad (7)$$

The relationship between the refractive index n and the ratio of the carrier concentration to the effective mass *N/m** is given by [18].

$$n^2 = \varepsilon_L - \left[\frac{e^2}{4\pi^2\varepsilon_0 c^2}\right]\left[\frac{N}{m^*}\right]\lambda^2 \quad (8)$$

where *e* (1.6021 x $10^{-19}$ C) is the electronic charge, $c$ is the velocity of light, $\varepsilon_0$ is the permittivity of free space ($8.854\times10^{-12}$ F/m) and $\varepsilon_L$ is lattice dielectric constant. From the intercept, the high-frequency dielectric constant, $\varepsilon_\infty = n^2$ equals 3.09. It is clear that $\varepsilon_L > \varepsilon_\infty$ by 0.03, and this result is attributed to the small concentration contribution of free carriers for polarization. The dielectric constant of a material can be calculated using the dispersion relation of incident photon. The refractive index was also fitted using a function for extrapolation towards shorter wavelengths [22]. The model of Moss stated that the free carriers contribution to dispersion are relatively small. This means that data corresponding to the wavelength range lying below the absorption edge of the material are to be used. In such a case, one can apply the next relation. The properties of the investigated sample could be treated as a single oscillator at wavelength $\lambda_0$ at high frequency. The high frequency dielectric constant can be calculated by applying the following simple classical dispersion relation [23]:

$$\frac{n_0^2 - 1}{n^2 - 1} = 1 - \left(\frac{\lambda_0}{\lambda}\right)^2 \quad (9)$$

where $n_0$ is the refractive index at infinite wavelength $\lambda_0$ (average interband oscillator wavelength), *n* the refractive index and $\lambda$ the wavelength of the incident photon. Plotting $(n^2 - 1)^{-1}$ against $\lambda^{-2}$ which showed linear part, was below the absorption edge as shown in Fig.8.

Simple empirical relation based on generalized Miller's rule can be used for the estimation of the nonlinear refractive index , $n_2$ , and susceptibility, $\chi^3$ . The nonlinear refractive index and susceptibility can be calculated by combining Miller's generalized rule [24–27] and low-frequency linear refractive index estimated from Wemple–DiDomenico single effective oscillator model. The third-order nonlinear optical susceptibility, $\chi^{(3)}$ , is an important parameter, because it gives a measure about the possibility of using the films in optical switching. Due to fast response time on laser excitation and large value of the third order nonlinear susceptibility, semiconductors thin films are of considerable

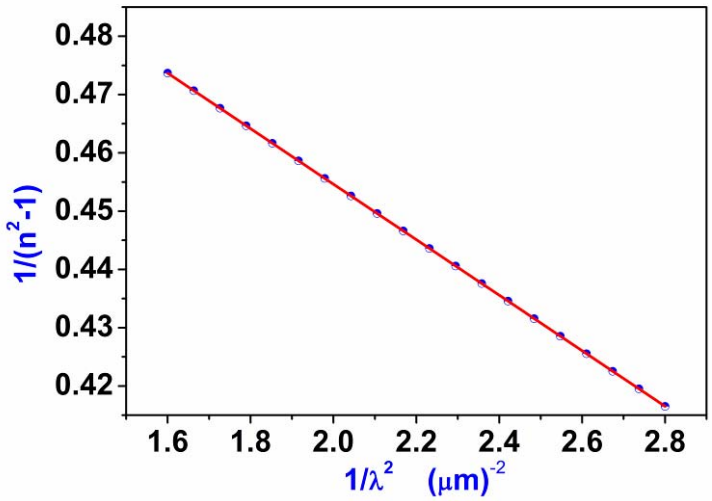


**Fig. 8.** The $1/(n^2 -1)$ versus $1/\lambda^2$ plot for POMA

interest [28]. The Miller rule provides a convenience and straight evaluation of third-order nonlinear susceptibility for visible, nonlinear and near infrared frequencies [29, 30]. It relates the third order of nonlinear polarizability parameter and the linear optical susceptibility , $\chi^{(1)}$, through the equation [22]:

$$\chi^{(3)} = A(\chi^{(1)})^4 = A/(4\pi)^4 (n-1)^4 \qquad (10)$$

where A = 1.7x10$^{-10}$ (for $\chi^{(3)}$ in esu ) .The magnitude of nonlinearity is mainly affected by surface roughness and charge carrier density of the films [31,32]. Fig.9 illustrates third order nonlinear optical susceptibility $\chi^{(3)}$ of the film as a function of photon energy hv. The obtained values are in the same range as reported for other thin films [33, 34]. It is obvious from Fig. 9 that $\chi^{(3)}$ increases with increasing wavelength. This trend can be ascribed to increase in carrier concentration which may lead to higher $\chi^{(3)}$ values by additional charge density polarization. The rough surfaces scatter more light from the fundamental beam and generate low nonlinear optical response [35].

The $n_2$ can be calculated from the relation [27]

$$n_2 = \frac{12\pi\chi^3}{n_0} \qquad (11)$$

The calculated values of nonlinear optical susceptibility $\chi^{(3)}$ and nonlinear refractive index , $n_2$, according to equations 10 and 11 are shown in table 1.

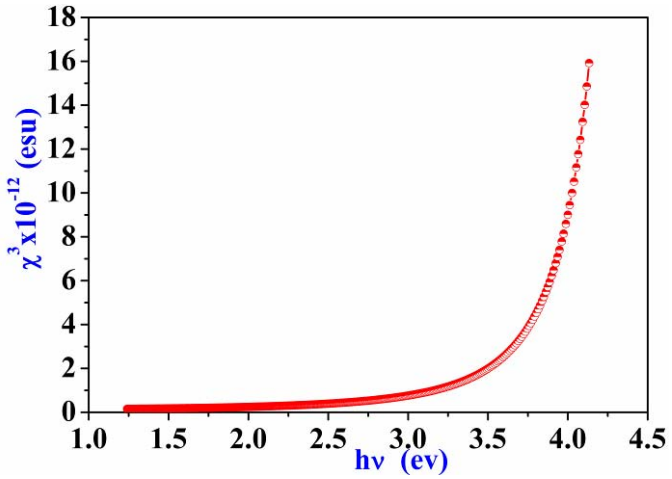


**Fig. 9.** Nonlinear optical susceptibility $\chi^{(3)}$ of POMA thin film as a function of photon energy hv.

**Table 1.** Optical parameters of POMA polymer

| $E_0$ (eV) | $E_d$ (eV) | $E_{gf}$ (eV) | $E_{go}$ (eV) | $\varepsilon_\infty$ | $\varepsilon_L$ | $n_0$ | $M_{-1}$ | $M_{-3}$ $(eV)^2$ | $S_0$ x$10^{+12}$ ($m^{-2}$) | $\chi^{(3)}$ x$10^{-13}$ (esu) | $n_2$ x$10^{-15}$ ($cm^2$/W) |
|---|---|---|---|---|---|---|---|---|---|---|---|
| 4.918 | 10.03 | 3.15 | 1.61 | 3.09 | 3.12 | 1.76 | 2.08 | 0.086 | 53 | 1.3 | 1.16 |

## 5. The Electrical properties of POMA polymer

Interdigitated electrodes (IDE) assembled from two individually addressable interdigitated comb-like electrode structures have frequently been suggested as ultra sensitive for chemical structure films. Interdigitated electrode structure with feature size in the nanometre scale is popular in the solid-state physics [36]. The POMA thin films were synthesized by using spin coating method. The polymer is dissolved in formic acid and deposited on either interdigitated finger electrode, or n-Type silicon wafer substrates. Fig.10 shows electrode that consists of interdigitatted Aluminium lines on a glass substrate was prepared according to Kareema. M. Ziadan *et al* [37]. It can be achieved using interdigitated electrodes to measure the surface conductivity of the samples from the following relationship [38].

$$\sigma_s = \frac{I}{V}\left(\frac{L}{Wt\ell}\right) \qquad (12)$$

where, $t$ is thickness of polymer, $W$ is the distance fingers, $\ell$is number of fingers, and $L$ is the space between electrodes ($L$=100μm).

**Fig. 10.** A schematic diagram of interdigitated finger electrode [37].

Fig. 11 shows the relation between logI and LogV for polymer POMA thin films at temperature (293-383) K. The thickness of the POMA polymer was 87.66 nm. The curve indicats ohmic behaviour.

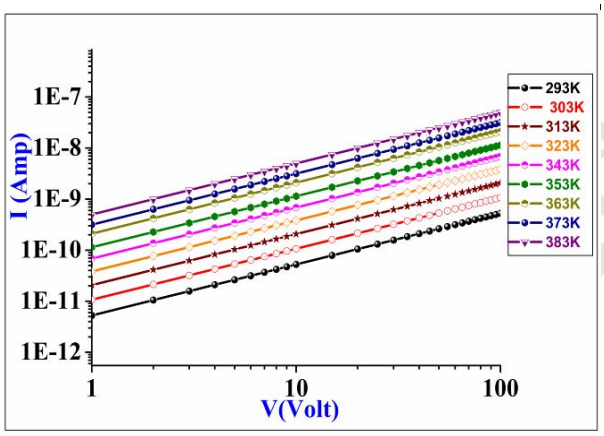


**Fig.11**. Current-Voltage characteristic for POMA at different temperatures .

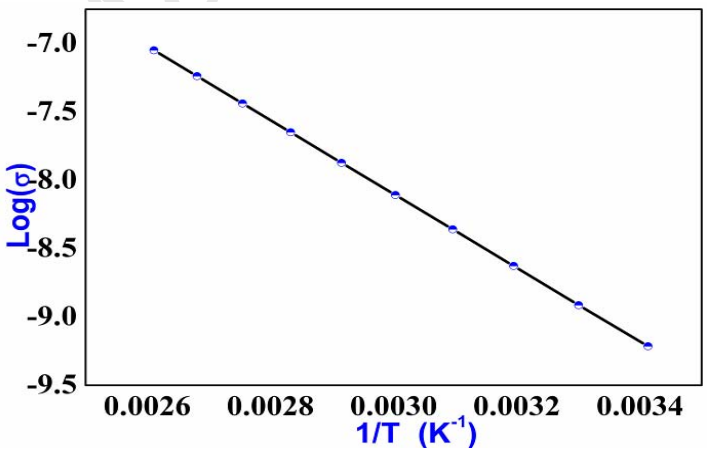


**Fig.12**. Log(σ) as a function of (1/T) for POMA.

Fig.12 shows the relation between logσ and 1/T $K^{-1}$ for POMA polymer thin films at temperature 293-383 K. The thickness of the POMA polymer was 87.66 nm. The electrical conductivity varied from $6.1x10^{-10}$ $S.cm^{-1}$ at room temperature to $8.92x10^{-8}$ $S.cm^{-1}$ at temperature 383K. The polymer POMA shows semiconductor behavior [39,40]. The conductivity dependence on temperature for POMA films is shown in Fig.12. The temperature is enough to move the charge carriers from valence band to bipolaron state [41]. The conductivity follows the free carrier transition in the extending state over the chain length in addition to the inter chain transition . The activations energy for POMA films is greater than POT film that estimated the bipoloron state in POMA which is smaller than that created

in POT film [42]. Single layer solar cell prepared from POMA was deposited n-type silicon wafer Al/Si/POMA/Au as shown in Fig.13.

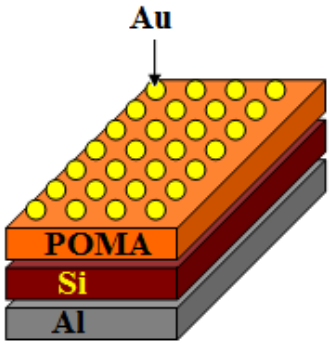


**Fig.13.** Single layer solar cells fabrication of POMA.

The gold (Au) electrode 20 nm in thickness was deposited on the top of sample, using the evaporation technique while Aluminum (Al) 90 nm in thickness was deposited as the back silicon using same evaporation technique. The evaporation method electrode was carried out in vacuum with low pressure of $10^{-4}$ –$10^{-5}$ torr. The energy conversion efficiency, $\eta$, is defined as the ratio of electrical power output of the cell at maximum point to the incident optical power $P_{in}$ and determined by the following equation:

$$\eta = \frac{output - power}{input - power} \times 100\% = \frac{P_{out}}{P_{in}} \times 100\% \qquad (13)$$

when ($P_{in}$=100mWcm$^{-2}$) is taken as the solar power incident on a unit area, the ratio between ($I_P V_P / I_{SC} V_{OC}$) called Fill Factor ($FF$) is a measure power that can get it from solar cell. It can be written in the following form when the current $I_P$ replaced by current density $J_{SC}$.

$$FF = \frac{J_P V_P}{J_{SC} V_{OC}} \qquad (14)$$

Where $J_P$ is maximum current density , $J_{SC}$ is short circuit current density, $V_P$ is maximum voltage and $V_{OC}$ is open circuit voltage. Thus [43],

$$\eta\,(\%) = \frac{V_{OC}.J_{SC}.FF}{P_{in}} \times 100 \qquad (15)$$

According to Eq. 15, it is clear that $J_{SC}$, $V_{OC}$ and $FF$ are important factors influencing the efficiency of POMA sensitized solar cells. However, it is still difficult to quantitatively characterize the

parameters affecting the *FF*, while key factors influencing $J_{SC}$ and $V_{OC}$ have been widely discussed. Fig. 14 shows the relationship between current and voltage in light and dark of photovoltaic devices based on configuration of type [Al/Si/POMA/Au] under 100mW/cm$^2$. The POMA layer provides an appropriate work function to form an ideal contact with the active layer and a smooth surface over Al to avoid pin holes and the relevant parameters were summarized in Table 2.

**Table 2.** Photovoltaic parameters of Al/Si/POMA/Au solar cell.

| d nm | $V_{oc}$ (V) | $J_{sc}$ (Am/cm$^2$) | $V_p$ (V) | $J_p$ (mA/cm$^2$) | $P_{max}$ (mW/cm$^2$) | FF | η | R (Ω) | $R_{sh}$ (Ω) |
|---|---|---|---|---|---|---|---|---|---|
| 35 | 0.33 | 3.4 | 0.2 | 2 | 400 | 0.356 | 0.4 | 796.2 | 9554 |

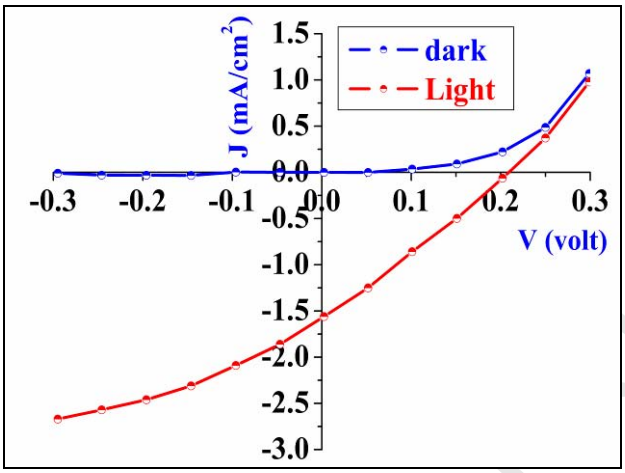


**Fig. 14.** J-V curves of solar cell device tested under 100 mW/cm$^2$

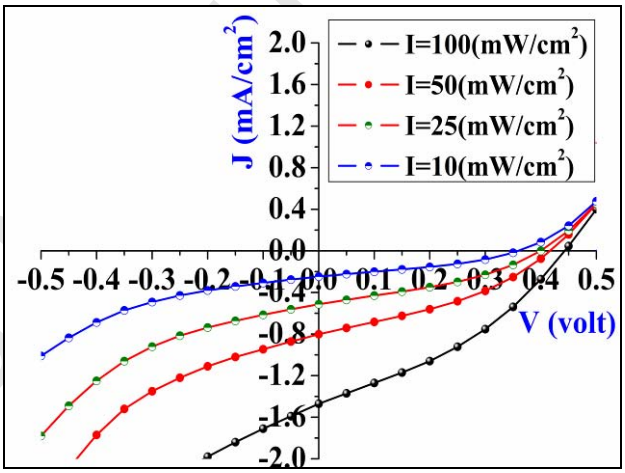


**Fig. 15.** J-V curves of solar cell device tested at different light intensity.

Fig. 15 shows the current density *J* as a function of the voltage with illumination through light intensity of 10, 25, 50, and 100 mW/cm$^2$. The thickness of POMA was 35 nm. The parameters of solar cells tabulated at table 3. The current density increases with the increase of illumination intensity. The table shows the dependence of the $V_{oc}$ on the intensity of incident light. The $V_{oc}$ increase slightly with intensity. While the short-circuit photo-current and the fill factor increases with illumination intensity, as well as, the power maximum grows with the increasing illumination intensity. The efficiency value reaches its maximum value 0.65 at 25 mW/cm$^2$ and then decreases at higher intensity 100 mW/cm$^2$ due to the effect of series resistance. Similarly Levitsky and coworkers observed the efficiency value that reached a maximum at 20 mW/cm$^2$ and then decreases at higher intensity 100 mW/cm$^2$ [44]. Riedel *et. al* also observed the efficiency that reaches its highest value at 5 mW/cm$^2$ and decreases by

more than 29-100 mW/cm$^2$ [45]. 'kink' was observed in the other reports [46-48] and was explained recently in a theoretical study [49].

**Table 3 .** Photovoltaic parameters of Al/Si/POMA/Au solar cell at different intensity.

| $P_{in}$ (mW/cm$^2$) | $V_{oc}$ (V) | $J_{sc}$ (Am/cm$^2$ ) | $V_p$ (V) | $J_p$ (mA/cm$^2$) | $P_{max}$ (mW/cm$^2$) | *FF* | $\eta$ |
|---|---|---|---|---|---|---|---|
| 100 | 0.45 | 1.5 | 0.26 | 0.8 | 208 | 0.338 | 0.208 |
| 50 | 0.41 | 0.7 | 0.24 | 0.6 | 144 | 0.501 | 0.252 |
| 25 | 0.4 | 0.5 | 0.25 | 0.65 | 162.5 | 0.812 | 0.65 |
| 10 | 0.35 | 0.25 | 0.19 | 0.15 | 28.5 | 0.325 | 0.285 |

## 6. Antibacterial activity

POMA pretense to have strong anti-bacterial activity against gram-negative and gram-positive bacteria including multidrug resistant strains. In the present study antibacterial activity of the POMA against different human pathogens is shown in Fig.16. It is apparent that the POMA showed inhibition zone against almost all the test organism, namely Staphylococcus aureus (SA), Escherichia coli (EC), Streptococcus pyogenes, Klebsiella pneumoniae, and Proteus mirabilis. The organisms were cultured on maintenance media until use and stored at 4°C. Inoculum was prepared using standard protocol M7-A7-CLSI with suitable modifications. In which bacterial cultures were grown on nutrient agar plates and maintained on the nutrient agar slants at 4°C. 4-5 well isolated colonies of the same morphological type were selected from an agar plate culture and transferred into a tube containing 5-6 ml of nutrient broth medium. The broth culture was incubated at 37 °C for 24 hrs. The turbidity of inoculum was compared with 0.5 McFarland standards, containing 1-2 x10$^8$ cfu/ml. The antimicrobial activity of POMA was evaluated by agar disk diffusion assay [50]. Muller Hinton Agar (MHA) plates were prepared for testing antibacterial activity. The prepared inoculum of bacteria was spread on plates (100 µl). Wells were made and filled with 30 µl of conducting polymer in a concentration of 50 mg/ml each MHA plates were incubated at 37°C for 24 hours. After incubation the zone of inhibition was measured using Hi antibiotic zone scale. The experiment was carried out in triplicates and standard deviation calculated. The size of inhibition zone was different according to the type of bacteria. The inhibition zone is found to be more for gram negative bacteria than gram positive bacteria. The antimicrobial mechanism of this conducting polymer is still unclear, and is under investigation. It has been proposed that the antimicrobial activity of aniline-based conducting polymers took effect through electrostatic adherence between polymer molecules and bacteria, leading to the destruction of the bacterial cell walls, and thus death of the bacteria [51].

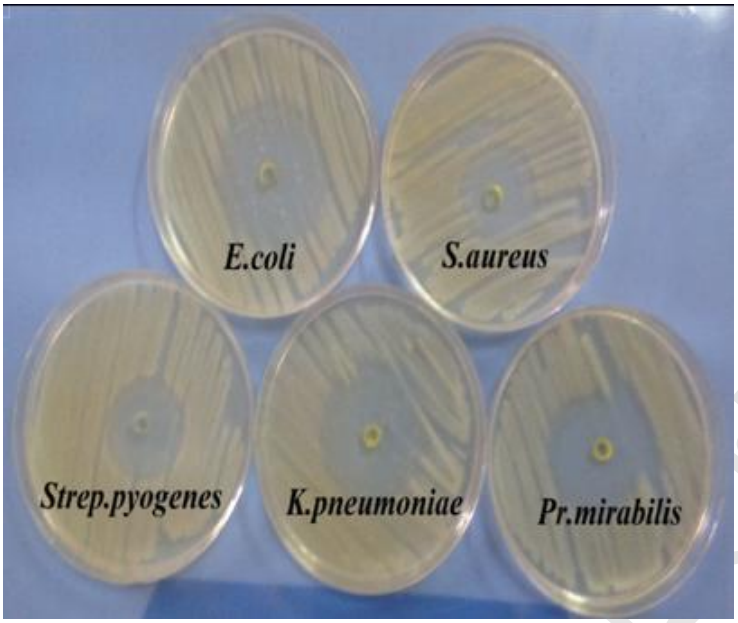


**Fig. 16.** Photograph showing antibacterial activity against Staphylococcus aureus (SA), Escherichia coli (EC), Streptococcus pyogenes, Klebsiella pneumoniae and Proteus mirabilis.

Fig. 16 shows the antibacterial effect of the conducting polymer. The highest mean zone of inhibition (40 mm) is recorded for conducting polymer POMA against the gram negative bacterium Esherichia coli , 38.5 mm is observed for 50 mg/mL of POMA against Proteus mirabilis while the minimum zone of inhibition was found to be 32.5 mm in diameter against Streptococcus pyogenes as shown in Fig.17. It is worth noting that the ability of the conducting polymer to act as an electron donor or electron acceptor is central to both free radical scavenging and antimicrobial activity. It is also possible that conducting polymer not only interact with the surface of membrane, but can also penetrate inside the bacteria.

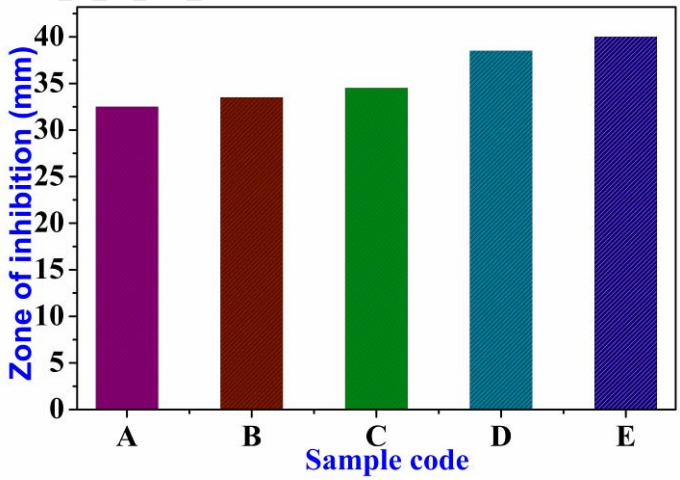


**Fig. 17**. The size of the zone of inhibition formed around each disc, (A) *Streptococcus pyogenes*, (B) *Staphylococcus aureus*, (C) *Klebsiella pneumonia* (D) *Proteus mirabilis*,(E) *Escherichia coli*.

## 7. Nonlinear studies of dye doped POMA

Both nonlinear refraction and nonlinear absorption in solid and liquid samples can be rapidly measured by the Z-Scan technique, which utilizes self-focusing or self-defocusing phenomena in optical nonlinear materials. For this study we have prepared dye solution and thin film. The solution sample of the dye orcein was dissolved in N-methyl-2-pyrrolidone (NMP). The concentration of the dye solution is 0.5 mM. To prepare the solid films, POMA was selected as the host material because it is hard and rigid. A known quantity of POMA and orcein were dissolved in NMP separately, the concentration of the orcein in NMP is 0.5 mM, later both solutions were mixed and stirred for 2 hr using a magnetic stirrer. The ratio of POMA solution and dye solution is 1:1. The film was prepared on a clean glass slide by the casting method and dried at 20 $^0$C for 24 hrs. The film sample has a good purity and uniform thickness. The thickness of the film was measured using digital micrometer and is found to be 15μm. The Z-scan technique was applied for the measurements of nonlinear optical characteristics of investigated samples. We used a SDL laser beam with 532 nm wavelength and power of 40 mw, which was focused by (+5cm) focal length lens. The laser beam waist $\omega_0$ at the focus measures 21.63 μm and the Rayleigh length measured $Z_R$= 2.76 mm. A 1 mm thickness optical cell containing the dye in NMP is translated across the region along the axial direction of the laser beam propagation. The transmission of the beam through an aperture placed in the far field was measured using a photo detector fed to a power meter. For the open aperture Z-scan, a lens was used to collect the entire laser beam transmitted through the sample replaced the aperture. Fig. 19 shows the closed aperture Z-scan data for 0.5 mM concentration of dye solution in NMP and polymer film at incident intensity $I_0$ =5.44 kW/cm$^2$. The scan of both the samples has peak-valley configuration, corresponding to negative nonlinear refraction index, i.e. self-defocusing occur. The defocusing effect is attributed to a thermal nonlinearity resulting from the absorption of a tightly focused beam traversing through the absorbing medium that produces spatial distribution of the temperature in the sample and, consequently, a spatial variation of the refractive index that acts as a thermal lens resulting in phase distortion of the propagating beam.

Let $\Delta\phi_\circ$ be the on-axis phase shift at the focus of the lens which is related to the difference in the peak and valley transmission $\Delta T_{P-V}$ as [52]:

$$\Delta T_{P-V} = 0.406(1-S)^{0.25}\Delta\phi_\circ \qquad (16)$$

where $S = 1-\exp(-r_a^2/\omega_a^2)$ is the aperture linear transmittance (=0.41) with $r_a$ denoting the aperture radius and $\omega_a$ denoting the beam radius at the aperture in the linear regime. $\Delta\phi_\circ$, the onaxis phase shift is related to the third-order nonlinear refractive index by [53].

$$\Delta\phi_{\circ} = kn_2 L_{eff} I_{\circ} \qquad (17)$$

where $k=2\pi/\lambda$, $L_{eff} = (1-\exp(-\alpha L))/\alpha$ is the effective thickness of the sample, $\alpha$ the linear absorption coefficient, $L$ the thickness of the sample, $I_{\circ}$ the on-axis irradiance at focus and $n_2$ is the third-order nonlinear refractive index.

Fig. 18 shows the measured Z-scan data for open aperture set-up for the dye in solvent and polymer film. The typical Z-scan data with fully open aperture is insensitive to nonlinear refraction, therefore the data is expected to be symmetric with respect to the focus, but the absorption in the sample enhances the valley and decreases the peak in the closed aperture Z-scan curve and results in distortions in the symmetry of the Z-scan curve about Z=0. The nonlinear absorption coefficient βcan be estimated from the open aperture Z-scan data [54]

$$\beta = 2\sqrt{2}\Delta T / I_{\circ} L_{eff} \qquad (18)$$

where ΔT is one-valley transmission.

In general, the measurements of the normalized transmittance versus the sample position for the cases of the closed and open apertures allow for the determination of the nonlinear refractive index, $n_2$, and the nonlinear absorption coefficient β since the closed aperture transmittance is an effected by the nonlinear refraction and absorption. The determination of $n_2$ is less straight forward from the closed aperture scans. It is necessary to separate the effect of the nonlinear refraction from that of the nonlinear absorption. A method to obtain a purely effective $n_2$ is to divide the closed aperture transmittance by the corresponding open aperture scans [55]. The data obtained in this way purely reflects the effects of the nonlinear refraction. The ratio of Figs. 18 to 19 scans is shown in Fig. 20.

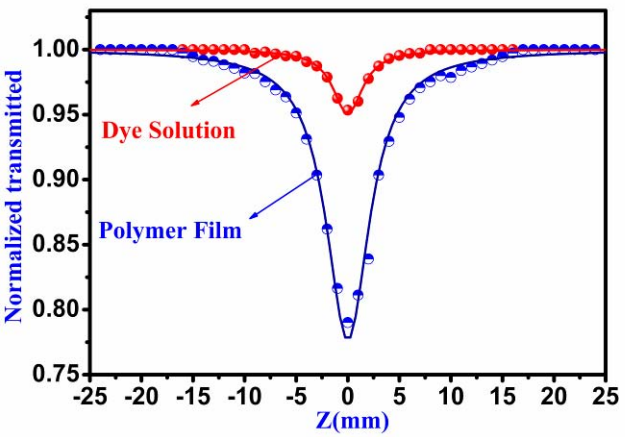


**Fig. 18.** Open-aperture Z-scan data

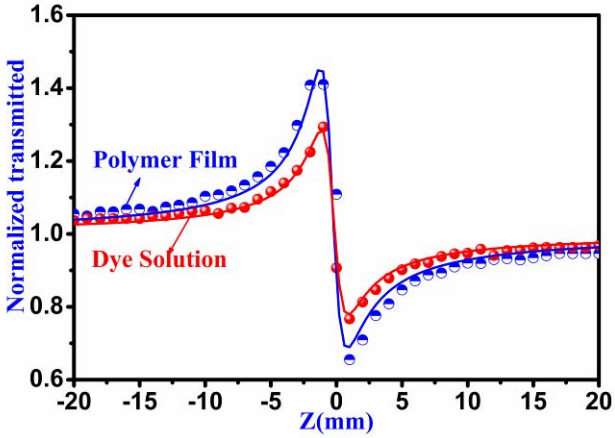


**Fig. 19.** Closed-aperture Z-scan data

The values of the nonlinear refractive index and nonlinear absorption for dye in solvent and polymer film are given in Table 4. The value of $n_2$ in a dye doped film is found to have large value than in the case of solutions, this may be attributed to three reasons, firstly absorption coefficient ($\alpha$) for the dye doped film is larger than in the case of dye solution, secondly the heat dissipation being faster in liquids as compared to that in a solid medium, thirdly it is due to Anderson localization of photons [56]. This is because of the strong scattering regime as the scattering mean free path of photons is less than in the case of liquids, so the localization of strong electromagnetic field inside the solid is responsible for the increase in nonlinearity in optical materials.

Table4: Nonlinear optical parameters for dye solution and POMA thin film.

| Sample | $n_2 \times 10^{-7}$ $(cm^2/W)$ | $\beta \times 10^{-3}$ $(cm/W)$ | $\Delta n \times 10^{-3}$ |
|---|---|---|---|
| Dye Solution | 0.833 | 4.26 | 0.480 |
| POMA Film | 14.87 | 71.77 | 8.097 |

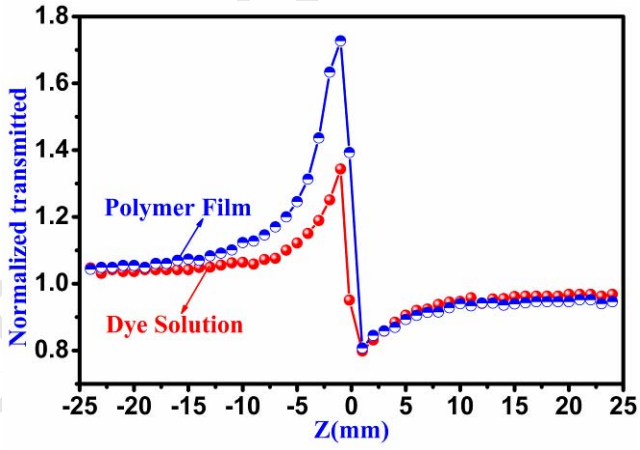


**Fig. 20.** Pure nonlinear refraction curves for dye solution and thin film.

## 8 . Conclusions

Conducting polymer, poly (*o*- methoxyaniline) (POMA), was chemically synthesized by the chemical polymerization method, hydrochloric acid (HCl) was used as dopant, under the same reaction conditions. We have fabricated photovoltaic devices using a new type material consisting a polymer poly (*o*- methoxyaniline) (POMA). The addition of POMA in the material can smoothen the film

surface morphology, reduce the occurrence of air pores and defects, enhance light absorption and can be used as an interfacial layer in organic solar cells application to minimize the reflectivity and improve the solar cells efficiency. The use of POMA in solar cells has great potential because POMA is abundant, thermally stable, and can be used in flexible devices. The recorded absorption spectra in the UV– vis region shows absorption bands and generally interpreted in terms of ($\pi - \pi^*$) excitation. Some of the important spectral parameters, namely optical absorption coefficient $\alpha$, high-frequency dielectric constant, $\varepsilon_\infty$, and the third-order nonlinear optical susceptibility, $\chi^{(3)}$, were calculated .The direct allowed transition was observed with band gap of 3.15 eV. The dispersion curve of the refractive index shows an anomalous dispersion in the absorption region and the dispersion parameters were obtained using single oscillator model. On the basis of band calculations, some of the optical constants of POMA film,i.e., the lattice dielectric constant and the oscillator parameter were evaluated. The presented optical investigation for POMA thin film gives evidence for the applicability of this compound in the field of optoelectronic devices. Further, conducting polymer has significant activity against Staphylococcus aureus, Escherichia coli, Streptococcus pyogenes, Klebsiella pneumoniae, and Proteus mirabilis with the zone of inhibition diameter 33.5, 40, 32.5, 34.5 and 38.5 mm respectively. The nonlinear optical response of the thermo-optic origin exhibited by the samples at low cw laser powers is studied using (SDL-532-100T). It was shown that the nonlinear absorption can be attributed to the reverse saturable absorption process, while the nonlinear refraction led to the self-defocusing in this conducting polymer.

**References:**

[1] P.C. Yang, J.Y. Sun, S.Y. Maa, Y.M. Shen, Y.H. Lin, C.P. Chen, C.F. Lin, Sol. Energ. Mat. Sol. C. 98 (2012) 351.

[2] K. Tvingstedt, O. Inganäs, Adv. Mater. 19 (2007) 2893.

[3] M. Mohammadi, N. Shahtahmasebi, M. Karimipour, R. Sarhaddi, Optical and Magneto optical Properties, 5( 2012) 2912.

[4] S. Gunes, H. Neugebauer, N. Serdar Sariciftci, Chem. Rev. 107 (2007) 1324.

[5] H. Hoppe, N. S. Sariciftci, J. Mater. Chem. 19 (2004) 1924.

[6] S. H.Deshmukh, D.K. Burghate, V. P.Akhare, V.S. Deogaonkar, P.T. Deshmukh, M. S. Deshmukh, Bulletin of materials Science 30 (2007) 51.

[7] H. Nshruoke, T. Kawaharamura, J. Korean physical Society 53 (2008) 3025.

[8] K. Mallick, M. Witcomb, M. scurrell, Platinum Metals Rev. 51(2007) 3.

[9] J. Sui, L. Zhang, H. Peng, J. Travas Sejdic, P. A. Kilmarthin, Nanotechnology 20 (2009) 415606.

[10] L. Zhang, H.Peng, J. Sui, C. Soeller, P. Kilmarthin, J. Travas Sejdic, J. Phys. Chem.C,113 (2009) 9128.

[11] J. C. Fatuch, M. A. Soto Oviedo, C. O. Avellaneda, M. F. Franco, W. Romao, M. A. De Paoli, A. F. Nogueira, Synth. Met. 159 (2009) 2348.

[12] X. Wang, S. Ray, M. Gizdavic Nikolaidis, A. J. Easteal, J. Polymer Science Part A: Polymer Chem. 50 (2012) 353.

[13] J. Tauc, Amorphous and Liquid Semiconductors, Plenum, New York, 1974.

[14] A. P. Singh, S. Kumari, R. Shrivastav, Int. J. Hydrogen Energy 33 (2008) 5363.

[15] D. Cahen, A. Kahn, E. Umbach, Mater. Today 8 (2005) 32.

[16] A. Y. Al-Ahmad, Q. M. A. Hassan, H. A. Badran, K. A. Hussain, Opt. & Las Tech. 44 (2012) 1450.

[17] M. Di Domenico Jr, S. H. Wemple, J. Appl. Phys. 40 (1969) 720.

[18] M. M. Abdel-Aziz, I. S. Yahia , L. A. Wahab, M. Fadel , M. A. Afifi, Appl. Surf. Sci. 252 (2006) 8163.

[19] H. A. Badran, M. F. AL-Mudhaffer, Q. M. A. Hassan, A. Y. AL-Ahmad, Chalcogenide Letters, 9 (2012) 483 .

[20] F. Yakuphanoglu, A. Cukurovali, I. Yilmaz, Physica B 351 (2004) 53.

[21] S.H. Wimple, M. Didomenico, Phys. Rev. Lett. 23 (1969) 1156.

[22] S. H. Wemple, M. Didomenico, Phys. Rev. B 3 (1971) 1338.

[23] T.S. Moss, Optical Properties of Semiconductors, Butter Worths Scientific Publication LTD., London (1959).

[24] C. Wang, Phys. Rev. 2 (1970) 2045.

[25] H. Ticha, L. Tichy, Journal of Optoelectron. Adv. Mater. 4 (2002) 381.

[26] J. Wyne, Phys. Rev. 178 (1969) 1295.

[27] R. Tintu, V.P.N. Nampoori, P. Radhakrishnan, S. Thomas, Opt. Commun. 284 (2011) 222.

[28] M. Alaoui Lamrani, M. Addou, Z. Sofiani, B. Sahraoui, J. Ebothe, A. El Hichou, N. Fellahi, J.C. Bernede, R. Dounia, Opt. Commun. 277 (2007) 196.

[29] H. A. Badran, A. Y. Taha, A. F. Abdulkader, C. A. Emshary, J. Ovonic Research 8 (2012) 161.

[30] K. Bahedi, M. Addou, M. El Jouad, Z. Sofiani, M. Alaoui Lamrani, T. El Habbani, N. Fellahi, S. Bayoud, L. Dghoughi, B. Sahraoui, Z. Essaidi, Appl. Surf. Sci. 255 (2009) 4693.

[31] H.Ticha, J.Schwarz, L.Tichy , R. Mertens, J. Optoelectron. Adv. Mater. **6,** 747 (2004).

[32] Z. Sofiani, B. Sahraoui, M. Addou, R. Adhiri, M. Alauoui Lamrani, L. Dghoughi, N. Fellahi, B. Derkowska, W. Bala, J. Appl. Phys. 101 (2007) 063104.

[33] R. Adair, L.L. Chase, S.A. Payne, Phys. Rev. B 39 (1989) 3337.

[34] V. Narayanan, R.K. Thareja, Opt. Commun. 260 (2006) 170.

[35] A. Abdolahzadeh Ziabari, F. E. Ghodsi, J. Mater. Sci: Mater. Electron. 23 (2012)1628.

[36] L. Skjolding, C. Spegel, A. Ribayrol, J. Emneus, L. Monteius, J. of physics, 100 (2008) 052045.

[37] K. M. Ziadan, Hussein. F. Hussein, K.I.Ajeel, Energy Procedia 18 ( 2012 ) 157 .

[38] A. J. Moulson, J. M. Herbe, "Electroceramics Materials, Properties ",Second Edition Materials, John Wiley & Sons Ltd, p. 9, (2003).

[39] V. Cherpak, P. Stakhira, Z. Hotra, O. Aksimentyeva, B. Tsizh, D. Volynyuk, I. Bordun, J. of Non-Crystalline Solids 354 (2008) 4282.

[40] F. Yakuphanoglu, I. Erol, Y.Aydogdu, M. Ahmedzade, Mater. Lett. 57 (2002) 229.

[41] K. M. Ziadan " Electrical & optical properties of conducting polymers (PT, PT/ PTFE, PT/ PVC and application in rechargeable behavior" PhD thesis Basrah university, Iraq 1997.

[42] V. Shaktawat, N. Jain, M. Dixit, N. Saxena, K. Sharma,T. Sharma, Indian J. Pure & Applied Physics 46 (2008) 427.

[43] H. Gazy Lazim, K. I. Ajeel, Hussain A. Badran**,** Spectrochimica Acta Part A: Molecular and Biomolecular Spectroscopy 145 (2015) 598.

[44] I. A. Levitsky, W. B. Euler, N. Tokanova, J. Castracane, Appl. Phys. Lett. 85 (2004) 6245.

[45] I. Riedel, N. Martin, F. Giacalone, J. L. Segura, D. Chirvase, J. Parisi, V. Dyakonov, Thin Solid Films 451-452 (2004) 43.

[46] P. Peumans, S.R. forrest, Appl. Phys. lett. 79 (2001)126.

[47] D. Ma, Y. Hu, Y. Zhang, L. Wang, X. Jing, F. Wang, J. M. Lupton, I. D. W. Samuel, S. C. Lo, P. L. Burn, Synth. Met. 137 (2003) 1125 .

[48] P. Ravirajan, S. A. Haque, J. R. Durrant, D Poplavskyy, D. D.C. Bradley, J. Nelson, J. Appl. Phys. 95 (2004) 1473.

[49] J. Nelson, J. Kirkpatrick, P. Ravirajan. Phys. Rev. B. 69 (2004) 03537.

[50] S. Rezaei-Zarchi, A. Javed, M. Javeed Ghani, S. Soufian, S. Hossein Mirjalili, Iranian Journal of Pathology 5 (2010) 83.

[51] N. Shi, X. Guo, H. Jing, J. Gong, C. Sun, K. Yang, J. Mater. Sci. Technol. 22 (2006) 289.

[52] H. A. Badran, Adv. Phys. Theor. Applica. 26, (2013) 36.

[53] H. A. Badran ,Appl. Phys. B 119 (2015) 319.

[54] G. Vinitha, A. Ramalingam, Las Phy. 18, (2008) 37.

[55] M. Sheik-Bahae, A.A. Said, T.H. Wei, IEEE J. Quantum Electron. 26, (1990) 760.

[56] R. R. Krishnamurthy, A. Ramalingam, Opt Applicata, XL, (2010) 187.